Available online at www.sciencedirect.com
SCIENCE DIRECT®
Thermochimica Acta 416 (2004) 105–111
thermochimica acta
www.elsevier.com/locate/tca

Estimation of interlamellar water molecules in sphingomyelin bilayer systems studied by DSC and X-ray diffraction

M. Kodama [a,*], M. Abe [a], Y. Kawasaki [a], K. Hayashi [a], S. Ohira [a], H. Nozaki [a], C. Katagiri [b], K. Inoue [c], H. Takahashi [d]

[a] *Department of Biochemistry, Faculty of Science, Okayama University of Science, 1-1 Ridai-cho, Okayama 700-0005, Japan*
[b] *Biochemistry Laboratory, Institute of Low Temperature Science, Hokkaido University, Sapporo, Hokkaido 060-0819, Japan*
[c] *Japan Synchrotron Radiation Research Institute (JASRI), Kouto, Mikazuki-cho, Sayo-gun, Hyogo 679-5198, Japan*
[d] *Department of Physics, Gunma University, Aramaki 4-2, Maebashi 371-8510, Japan*

Received 11 December 2002; received in revised form 20 January 2003; accepted 29 January 2003

Available online 22 January 2004

Abstract

A study on the hydration property of lipid bilayer systems was performed with DSC and X-ray diffraction techniques for two sphingomyelins, a naturally occurring bovine brain sphingomyelin having a heterogeneous acyl chain and a semisynthetic sphingomyelin having the acyl chain of 16 saturated carbons. The number of differently bound interlamellar water molecules was estimated for the two sphingomyelin systems from a deconvolution analysis of the ice-melting DSC curves of varying water content. The estimated limiting, maximum number of freezable interlamellar water molecules for the semisynthetic sphingomyelin system was 5.5 H_2O per molecule of lipid, which is close to a value (5 H_2O/lipid) previously reported by us for a system of dipalmitoylphosphatidylcholine. However, for the brain-sphingomyelin system, a limiting hydration for this type of water was not reached even up to the water/lipid molar ratio ∼20. In this accord, the electron density profile analysis of X-ray lamellar diffraction patterns for the brain–SM system showed that the thickness of interlamellar water layer increases in proportion to the amount of added water.

Keywords: Sphingomyelin; Interlamellar water; DSC; X-ray diffraction

1. Introduction

Phospholipids are major components of biomembranes and are classified into two types, glycerolipid and sphingolipid, according to their backbone moiety, glycerol or sphingosine (Fig. 1). Sphingomyelin (SM) is a typical sphingophospholipid and comprises a phosphorylcholine head group; this head group is the same as that of diacylphosphatidylcholine (PC) which is the most abundant glycerophospholipid in biomembranes. The SM is composed of two different chains, a sphingosine chain and an amide-linked acyl chain, in contrast to two acyl chains for the case of PC. Although the SM is a minor phospholipid constituent in biomembranes, its specific functional role has been the subject of many investigations. In this connection, much attention has been given to hydrogen bonding groups of the SM molecule, compared with those of the PC molecule. Thus, the SM molecules contain both a hydroxyl group and an amide group acting as a hydrogen bond donor and acceptor [1], while the PC molecules have two carbonyl ester groups which function only as a hydrogen bond acceptor.

A naturally occurring SM is characterized by fairly differing acyl chain-length ranging from 14 to at least 24 carbons [2–6]. So, there is a mismatch in the length between the acyl chain and the sphingosine chain that is mostly 18 carbons long. Such a mismatch for the natural SM would be expected to cause a rough bilayer interface. From this viewpoint, in this study, the hydration property of lipid bilayer systems was investigated using DSC and X-ray diffraction techniques for two sphingomyelins, a naturally occurring bovine brain sphingomyelin having heterogeneous acyl chain (brain–SM) and a semisynthetic sphingomyelin having the homogeneous acyl chain of 16 saturated carbons (C16–SM). The number of differently bound water molecules existing in regions between bilayers was estimated from a deconvolution anal-

* Corresponding author. Fax: +81-86-255-7700.
E-mail address: kodama@dbc.ous.ac.jp (M. Kodama).

0040-6031/$ – see front matter © 2003 Elsevier B.V. All rights reserved.
doi:10.1016/j.tca.2003.01.003

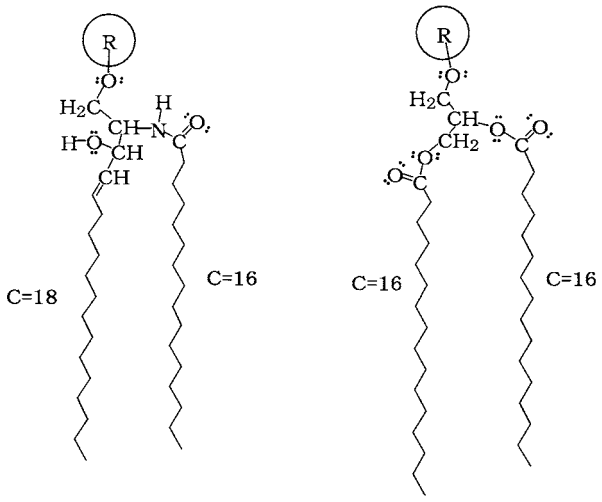

(a) *N*-palmitoylsphingomyelin (C16-SM) (b) dipalmitoylphosphatidylcoline (DPPC)

Fig. 1. Structures of *N*-palmitoylsphingomyelin (C16–SM)(a) and dipalmitoylphosphatidylcholine (DPPC)(b). R is a phosphorylcholine headgroup.

ysis of the ice-melting DSC curves of varying water content [7–12] and was compared for the brain–SM–water and the C16–SM–water systems. Furthermore, for the brain–SM system, the thickness of interlamellar water layer was estimated from the electron density profile analysis of X-ray diffraction patterns obtained for the lamellar phase.

2. Experimental

2.1. Materials

Two SMs were purchased from Sigma Co. (St. Louis, MO). One is a naturally occurring bovine brain SM having a heterogeneous acyl chain (~99% pure), denoted as brain–SM. The other is a semisynthetic SM having an acyl chain of saturated 16 carbons prepared from brain–SM (~97% pure), denoted as C16–SM.

2.2. Electrospray ionization mass spectrometry (ESI/MS) analysis for the acyl chains of brain–SM

The heterogeneous acyl chain of brain–SM was analyzed by ESI/MS performed with a JMS-LC mate instrument (JEOL, Japan) [2,3]. The mass of molecular species for the brain–SM was determined with positive ESI spectra for molecular ion adducts found at $[SM + Na]^+$ ($[SM + 23]^+$) and was then used to estimate both the total carbon number and the total double bond number given for the sphingosine chain plus the acyl chain. Subsequently, by assuming that all the sphingosines are 18:1 (= carbon number: double bond number), both the carbon and double bond numbers of the acyl chain were calculated for the respective molecular species. These results are given in Table 1 together with the composition of these molecular species. The average molecular weight estimated for the brain–SM is 776 and is consistent with a value reported by Untracht and Shipley [4]. Also, the acyl chain composition obtained in this study is very close to that reported by Kerwin et al. for a Sigma brain–SM [2].

2.3. Sample preparation

The brain–SM (approximately 30 mg) in a high pressure crucible cell for a Mettler DSC apparatus was dehydrated under high vacuum (10^{-4} Pa) at room temperature for at least 3 days until no mass loss was detected by electroanalysis

Table 1
Molecular mecies of the brain–SM

m/*z*	CN:DBN[(a)] for sphingosine plus acyl chain	CN:DBN[(b)] for acyl chain	Composition (mol %)
675	32:1	14:0	2.3
701	34:2	16:1	2.9
703	34:1	16:0	6.6
729	36:2	18:1	3.9
731	36:1	18:0	12.8
757	38:2	20:1	3.0
759	38:1	20:0	2.9
773	39:1	21:0	2.7
783	40:3	22:2	3.2
785	40:2	22:1	4.3
787	40:1	22:0	5.0
799	41:2	23:1	4.1
801	41:l	23:0	3.9
811	42:3	24:2	3.1
813	42:2	24:1	34.0
815	42:1	24:0	5.1

Average molecular weight for the brain–SM:776.
[(a)] Double bond number for sphingosine chain plus acyl chain.
[(b)] Double bond number for acyl chain estimated with sphingosine chain 18:1.

(Cahn Electrobalance). The crucible cell containing the dehydrated brain–SM was sealed off in a dry box filled with dry N_2 gas and was then weighed with a microbalance. The brain SM–water samples of varying water content were prepared by successive additions of the desired amount of water to the same dehydrated brain–SM with a microsyringe. Thus, only the weight of water was changed throughout the preparation of a series of the samples of varying water content up to the water/lipid molar ratio, N_w, ~20. After each addition of water, the samples were weighed with the microbalance and were annealed with a Mettler calorimeter by repeating thermal cycling (scanning rate of 0.2 °C/min) at temperatures above and below the gel-to-liquid crystal phase transition until the same transition behavior was attained. A series of the C16–SM-water samples of varying water content were prepared by the same procedure as that used for the brain–SM–water samples.

For the X-ray diffraction measurements, four brain–SM–water samples at N_w values 8.2, 10.1, 12.3, and 15.8 were prepared with the high pressure crucible cell in the same manner described above, respectively, and were transferred to an X-ray sample cell noted below.

2.4. Differential scanning calorimetry (DSC)

DSC was performed with a Mettler TA-4000 apparatus for the sample in the high pressure crucible cell (pressure resistant to 10 MPa) and on heating from −60 °C to temperatures of the liquid crystal phase at a rate of 0.5 °C min^{-1}.

2.5. X-ray diffraction

X-ray diffraction measurements were performed with an X-ray scattering spectrometer installed at BL40B2 of 8 GeV synchrotron radiation source of Japan Synchrotron Radiation Research Institute (JASRI). The details of the spectrometer have been described elsewhere [13]. X-ray diffraction patterns were recorded with a Rigaku R-AXIS IV imaging plate system. The area of the imaging plate was 30 cm × 30 cm. The X-ray wavelength was 0.100 nm and the sample-to-detector distance was 41.5 cm. The lipid samples were contained in the sample cell with a 2 mm path length and a pair of thin mica windows. The temperature of the sample was kept at 20 ± 0.5 °C using a thermostat. The exposure time was 180 sec. Two-dimensional data on imaging plate were integrated radially using FIT2D (Hammersley).

3. Results and discussion

3.1. Differential scanning calorimetry

In Fig. 2, a series of typical DSC curves is compared for the brain–SM–water (A) and the C16–SM–water samples (B) with increasing water content expressed in the water/lipid molar ratio, N_w. For the two series of the samples,

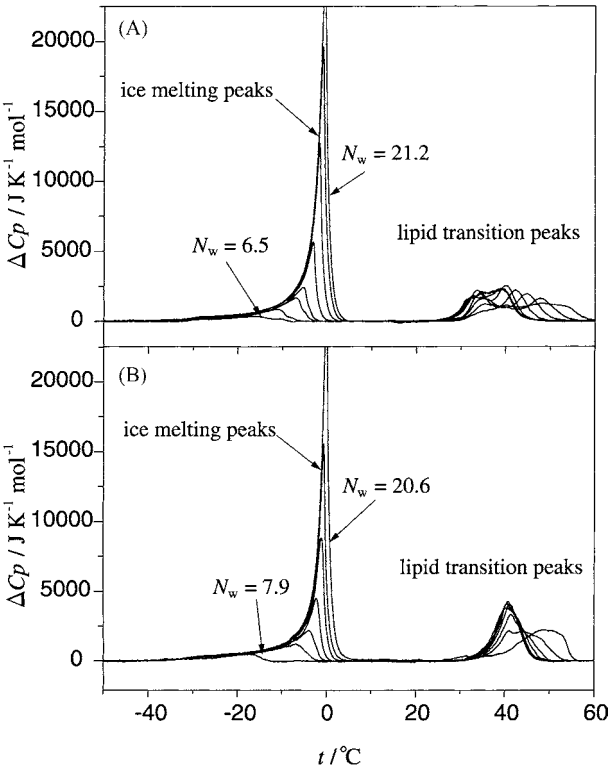

Fig. 2. Series of typical DSC curves for the brain–SM–water (A) and C16–SM–water systems (B). Water contents expressed in the water/lipid molar ratio (N_w) range from 6.5 to 21.2 for the brain–SM system (A) and from 7.9 to 20.6 for the C16–SM system (B), respectively.

the ice-melting DSC peaks are successively followed by lipid transition peaks of the gel (L_β)-to-liquid crystal phase transition, and so the melting behavior is attributed to the water molecules of the gel phase [7–11].

In Fig. 3, enlarged scale ice-melting peaks are compared for the two series of gel samples. The ice-melting peaks are composed of two components, broad and sharp, and their growth process with increasing water content is similar to that previously reported by us for various glycerophospholipid-water systems [7–11]. Thus, the broad components derived from freezable interlamellar water (i.e., the water existing in regions between the bilayers) begin to appear at around −40 °C, and grow in similar shapes without superimposing on one another. After that, the sharp components derived from bulk water (i.e., the water existing outside the bilayers) appear at around 0 °C and continue to grow up to N_w ~20. The sharp components of the brain–SM system shown in Fig. 3A occupy larger parts of their area at temperatures below 0 °C (dashed lines), compared with the C16–SM system shown in Fig. 3B. In other words, the temperature axis of the sharp components for the brain–SM system is shifted by 2–3 °C to the lower temperature side.

A deconvolution was performed with a computer program for multiple Gaussian curve analysis [9]. In the present deconvolution, both the half-height width (i.e., giving van't Hoff enthalpy) and the midpoint temperature

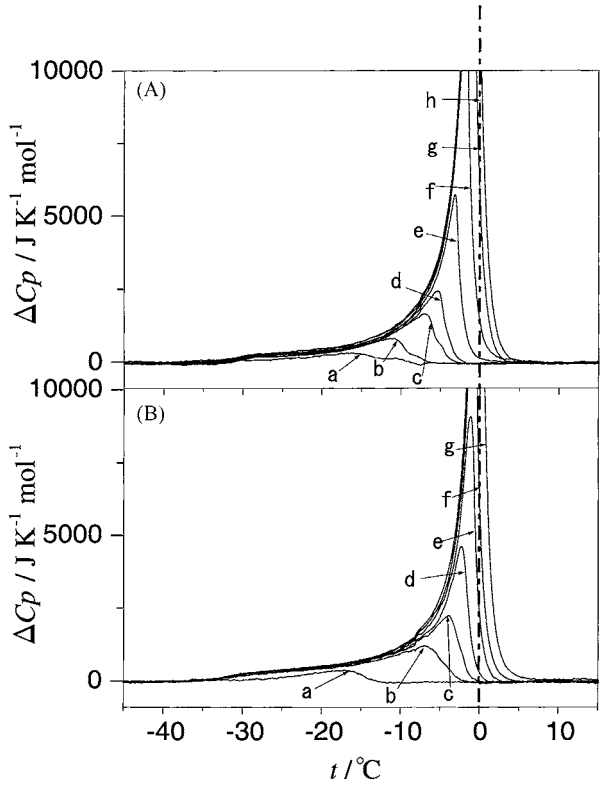

Fig. 3. Enlarged scale ice-melting DSC curves for the gel phase of the brain–SM-water (A) and C16–SM-water systems (B). The temperature axis at 0 °C is shown by hatched lines. N_w for the brain–SM system: a, 6.5; b, 8.1; c, 9.5; d, 10.2; e, 12.1; f, 15.1; g, 18.5; h, 21.2. N_w for the C16–SM system: a, 7.9; b, 9.2; c, 10.5; d, 12.1; e, 14.2; f, 16.7; g, 20.6.

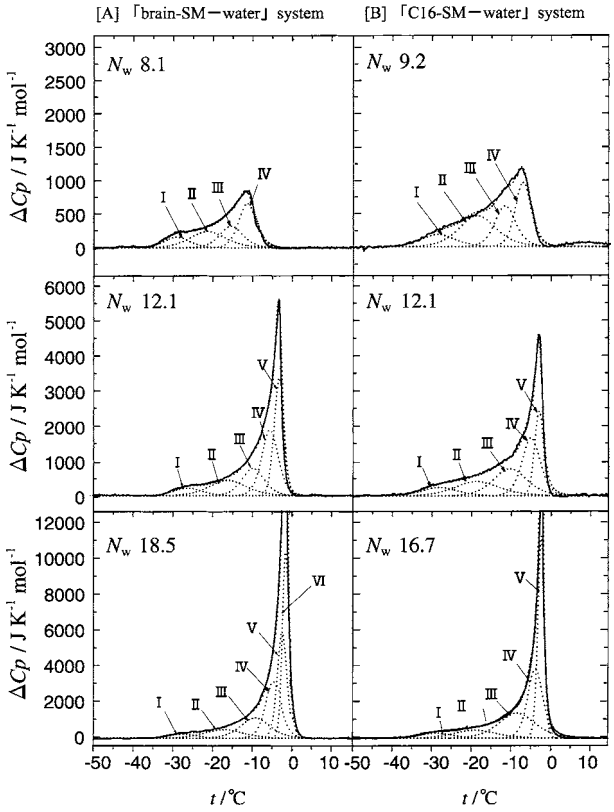

Fig. 4. Deconvolution analysis of ice-melting DSC curves for the gel phase of the brain–SM–water (A) and C16–SM–water systems (B) of varying water content. N_w values are indicated in this figure. The deconvoluted curves (I–VI) for the brain-system and the deconvoluted curves (I–V) for the C16–SM system are shown by dotted lines, together with their sum (the theoretical curve). The DSC curves are shown by solid lines.

characterizing individual deconvoluted curves were fitted to all the ice-melting DSC peaks of varying water content (thus, these two factors are almost constant throughout all the deconvolutions for varying water content). In Fig. 4, typical results of the deconvolution analysis are compared for the brain–SM (A) and C16–SM systems (B) of varying water content. Deconvoluted curves and their sum (i.e., the best-fitted curve) are shown by dotted lines and are compared with the experimental DSC curves (solid lines). Since the ice-melting peak for the bulk water is characterized by a Gaussian curve at a midpoint temperature of 0 °C [9], deconvoluted curves VI (N_w 18.5 in Fig. 4A) and V (N_w 12.1 and 16.7 in Fig. 4B) for the brain–SM and C16–SM systems are derived from the bulk water, respectively. Accordingly, deconvoluted curves I–V in Fig. 4A are assigned to the freezable interlamellar water of the brain–SM system, while deconvoluted curves I–IV in Fig. 4B are to that of the C16–SM system. Thus, the number of deconvoluted curves for the freezable interlamellar water is greater by one component for the brain–SM system than for the C16–SM system. This fact indicates that the low temperature part in the sharp ice-melting peaks of the brain–SM system contains an additional component (the deconvoluted curve V) for the freezable interlamellar water.

In Fig. 5, the ice-melting enthalpies (per mole of lipid) of the individual deconvoluted curves for the freezable interlamellar water are plotted against N_w together with the sum of these enthalpies, $\Delta H_{I(f)}$, and the results are compared for the brain–SM (A) and C16–SM systems (B). As shown in Fig. 5, the linear increase of $\Delta H_{I(f)}$ with increasing water content is observed up to N_w ~12 for the brain–SM system and up to N_w ~10 for the C16–SM system. As previously reported by us [7,9], the nonlinear increase of $\Delta H_{I(f)}$ observed above these boundary N_w values is caused by the bulk water which appears even though the limiting, maximum amount of the interlamellar water is not yet reached. Accordingly, the slope of linear portion of $\Delta H_{I(f)}$ curve is characterized only by the freezable interlamellar water, and so gives an average molar melting enthalpy for this type of water. On this basis, the average molar melting enthalpy for the freezable interlamellar water was estimated from the slope of the straight $\Delta H_{I(f)}$ line obtained by a least squares method and was then used to calculate the number of freezable interlamellar water molecules. The estimated average melting enthalpy for the freezable interlamellar water is 5.451 kJ/mol H_2O for the brain–SM system and 5.067 kJ/mol H_2O for the C16–SM system, and both enthalpy values are smaller than

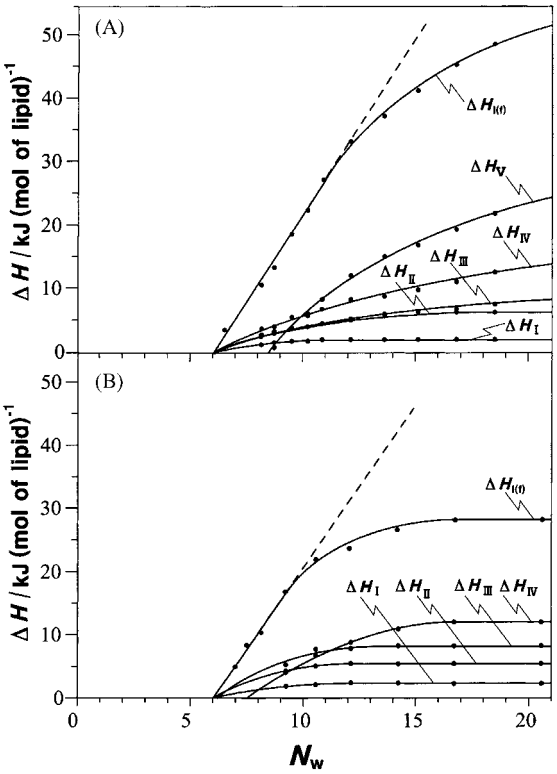

Fig. 5. Plots of ice-melting enthalpies for freezable interlamellar water versus N_w in the gel phase of the brain–SM–water (A) and C16–SM–water systems (B). $\Delta H_{I(f)}$ is the sum of the individual enthalpies of the deconvoluted curves for the freezable interlamellar water shown in Fig. 3.

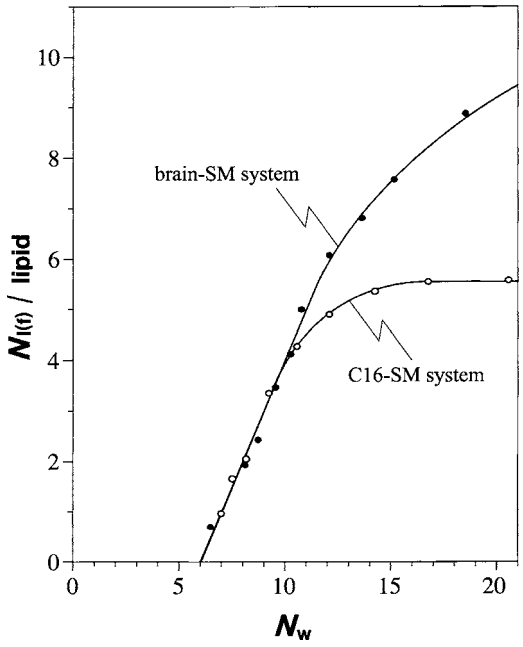

Fig. 6. Plots of the number of freezable interlamellar water molecules per molecule of lipid, $N_{I(f)}$, versus N_w for the gel phase of the brain–SM–water (●) and C16–SM–water systems (○).

the known melting enthalpy of hexagonal ice, 6.008 kJ/mol H_2O.

In Fig. 6, the estimated number of freezable interlamellar water molecules per molecule of lipid, $N_{I(f)}$, is plotted against N_w and is compared for the brain–SM and C16–SM systems. For N_w below ~10, the $N_{I(f)}$ curves for both systems can be expressed by the same linear line which intersects the abscissa at N_w ~6, indicating that the limiting, maximum number of nonfreezable interlamellar water molecules of these two SM systems is the same, i.e., 6 H_2O per molecule of lipid. For N_w above 10, the $N_{I(f)}$ curve of the C16–SM system reaches a maximum at N_w ~17, so giving the limiting, maximum number of freezable interlamellar water molecules of 5.5 H_2O per molecule of lipid (a full hydration of the gel phase of C16–SM system). However, for the brain–SM system, a limiting hydration is not yet reached even up to N_w ~20, and the number of the freezable interlamellar water molecules estimated at N_w 18.5 (final data in Fig. 6) is 9 H_2O/lipid, which is 1.6 times larger than the limiting value (5.5 H_2O/lipid) for the C16–SM system.

3.2. X-ray diffraction

Four samples of the brain–SM–water system at different N_w values 8.2, 10.1, 12.3, and 15.8 were examined at 20 ± 0.5 °C. The lamellar diffraction peaks were observed up to the 8th order for N_w 8.2 and were observed up to the 10th order for N_w values of 10.1 and 12.3. On the other hand, only four diffraction peaks were observed for N_w 15.8. Fig. 7 shows X-ray diffraction patterns for the sample at N_w 10.1. The lamellar spacing is 6.78 nm and is in agreement with a value previously reported by Untracht and Shipley for a bovine brain SM at similar water content [4]. As shown in Fig. 8, the observed lamellar spacings of these four samples increase linearly with increasing water content and the estimated slope is 0.109 nm/N_w. On the other hand, in the wide-angle regions shown in Fig. 7, a single peak appears at 1/0.42 nm^{-1}, indicating that the sample is in a gel state.

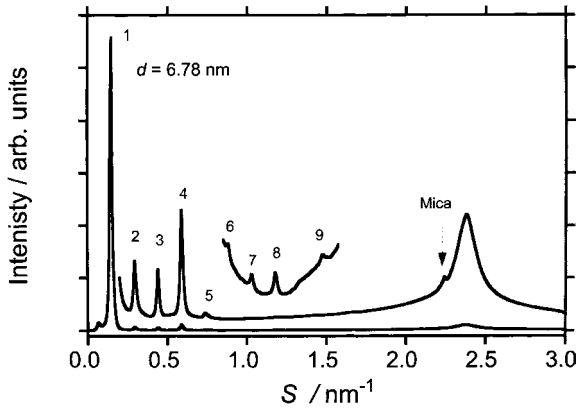

Fig. 7. X-ray diffraction patterns for the hydrated brain–SM at 20 °C (N_w 10.1). S is defined by $2\sin\theta/\lambda$, where 2θ is the scattering angle and λ is the wavelength of X-ray. For 0.2 < S, and 0.8 < S < 1.6, the plots with 20-fold and 500-fold expanded scales are also shown, respectively. The numbers in the figure indicate the order of the lamellar diffraction peaks.

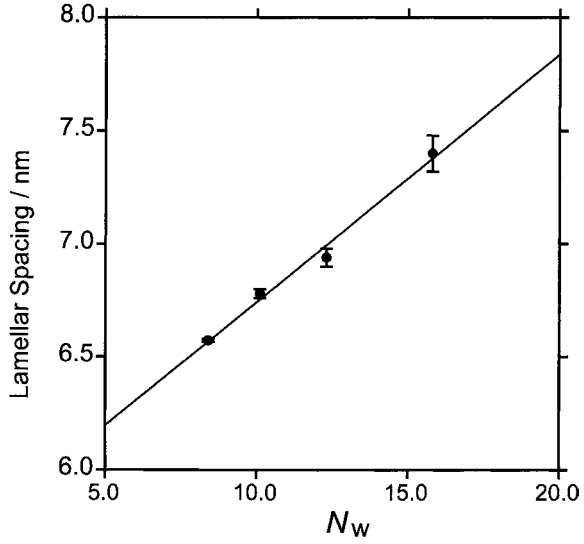

Fig. 8. Plots of observed lamellar spacing as a function of N_w. The errors are the standard deviations of the values estimated from each lamellar diffraction peak.

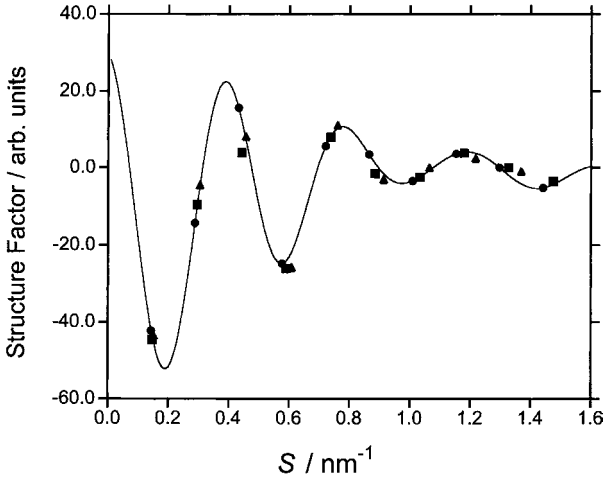

Fig. 9. Plots of the normalized structure factor for the hydrated brain–SM at 20 °C as a function of the reciprocal space (S). N_w: ▲, 8.4; ■, 10.1; ●, 12.3. The curve corresponds to the continuous Fourier transform calculated using the Shannon sampling theorem.

However, the peak is boarder than the lamellar diffraction peaks. This is caused by chain packing perturbations due to the heterogeneous acyl chains of brain–SM molecule given by Table 1. The wide-angle spacings were almost the same for all the samples.

For the samples that give rise to higher order lamellar diffraction peaks, i.e., for N_w values of 8.2, 10.1, and 12.3, we investigated further the bilayer structure by calculating electron density profiles. To calculate the electron density profiles, the observed lamellar diffraction intensities were corrected, normalized, and converted to structure amplitudes according to a method proposed by Worthington and Blaurock [14]. Phases of the diffraction peak were determined from the analysis of plots of structure amplitudes as a function of the reciprocal space (S), using the Shannon sampling theorem [15] (Fig. 9). The value of structure amplitude at zero of the reciprocal space was estimated by a method proposed by King and Worthington [16].

The calculated electron density profiles are displayed in Fig. 10. The troughs of profiles correspond to the bilayer center. Two peaks are assigned to the electron-rich phosphate headgroups for the apposing brain–SM molecules in an intrabilayer. The distance between the two peaks is about 5.1 nm. The positions of two peaks are almost the same for varying water content, indicating that the bilayer thickness of the brain–SM is constant within the hydration level examined in the present study. Accordingly, the linear increase in the lamellar spacing with increasing water content shown in Fig. 8 is due to an increase in the thickness of interlamellar water layers. Hence, the slope of Fig. 8 means the change ratio of water layer thickness against N_w. The result obtained by X-ray study is consistent with the calorimetric result such that the number of freezable interlamellar water molecules increases with increasing water content up to $N_w \sim 20$.

The present DSC and X-ray diffraction studies reveal that a limiting hydration of the brain–SM gel system is not reached even at N_w high enough to give a full hydration for the C16–SM gel system. As shown in Fig. 1a, the amide-linked palmitoyl and sphingosine chains of the C16–SM show structurally equivalent terminal ends in its molecule. This matching in the length between the two chains would provide a flat surface for the bilayer of C16–SM gel phase. Thus, the phosphorylcholine polar headgroup of C16–SM molecule would be expected to arrange horizontally at the bilayer interface. In this connection, the hydration property of the C16–SM gel bilayer obtained in this study is similar to that of the gel bilayer of dipalmitoylphosphatidylcholine (DPPC) having the same

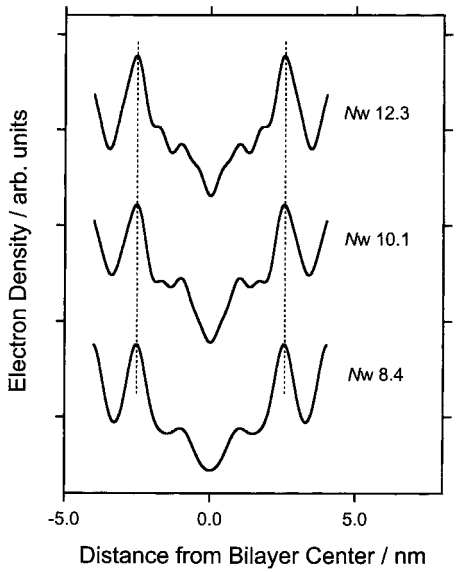

Fig. 10. Electron density profiles for the hydrated brain–SM at 20 °C.

phosphorylcholine head group and two palmitoyl chains (Fig. 1b) [9,11]. Actually, the limiting, maximum number of freezable interlamellar water molecules is 5.5 H_2O and 5 H_2O per molecule of lipid for the C16–SM and DPPC gel systems, respectively, and the average molar melting enthalpy for the freezable interlamellar water is 5.067 kJ and 5.025 kJ per mole of H_2O for the C16–SM and DPPC gel systems, respectively. Such a similar hydration property of the two phospholipids for the freezable interlamellar water suggests a critical contribution of the phosphorylcholine headgroups which form the flat bilayer surface at the interface.

However, the assumed flat bilayer surface would not be the case for the brain–SM gel system. This is because the length of the acyl chains of brain–SM is fairly different, as shown in Table 1. A point to be noted here is that the acyl chains of 24 carbons are much longer than the sphingosine chain (18 carbons). Also, the acyl chain of 14 carbons is shorter than the sphingosine chain. Considering the van der Waals interaction energy as a main determinant for the chain packings [17,18], the interdigitated packing would be energetically favorable for the two chains of brain–SM molecule [19–23]. Presumably, the packings are performed by the pairing of opposing brain–SM molecules in an intrabilayer, for example, in such a way that the longer acyl chain in one monolayer crosses the center of bilayer and comes into end-to-end contact with the shorter sphingosine chain in the other monolayer. For such interdigitated packings, the total carbon number for the two chains of the opposing molecules determines the chain-chain thickness of the bilayer. A pair between the SM molecules with 24-carbons acyl chain gives the total 42(=24 + 18) carbons in the longest case. The total 32 (=14 + 18) carbons in the shortest case are given by the pairing of the SM molecules of 14-carbons acyl chain. Referring the acyl chain distribution in Table 1, a pair of the SM molecules giving the total 41–42 carbons is found to occupy 50 mol%, and about 30 mol% is counted for a pair with the total carbon number smaller than 36. If a pair of the SM molecules with the large total carbon number distributes at random in an intrabilayer, a concavo-convex bilayer surface is assumed, so that the amide group and the hydroxyl group acting as a hydrogen bond donor and acceptor (Fig. 1a) would be directly exposed to interlamellar water. This would result in more enhanced hydration for the brain–SM system compared with the C16–SM system. Furthermore, if pairs of the SMs with relatively large total carbon number localize in the bilayer (this leads to a formation of domain structure), a water pocket would be created on the surface by the pairs of the SMs with the smaller total carbon numbers. This also could induce the enhanced uptake of the freezable interlamellar water for the brain–SM system. However, as shown in Fig. 10, the electron density profiles obtained in the present study could not reveal the interdigitated structure for the brain–SM gel system; they are similar to results for a natural SM previously reported by other workers [23]. In the past X-ray studies, the characteristic profiles due to the interdigitation have been reported only for systems of synthetic SM having an acyl chain longer than at least 22 carbons [19,22,23]. Since the X-ray diffraction technique gives average structural parameters, no evidence for the interdigitation could be obtained for the natural SMs characterized by the wide distribution of acyl chain-length because of their forming the rough bilayer surface as discussed above.

References

[1] I. Pascher, Biochim. Biophys. Acta 455 (1976) 433.
[2] J.L. Kerwin, A.R. Tuininga, L.H. Ericsson, J. Lipid Res. 35 (1994) 1102.
[3] W. Pruzanski, E. Stefanski, F.C. de Beer, M.C. de Beer, A. Ravandi, A. Kuksis, J. Lipid Res. 41 (2000) 1035.
[4] S.H. Untracht, G.G. Shipley, J. Biol. Chem. 13 (1977) 4449.
[5] W.I. Calhoun, G.G. Shipley, Biochim. Biophys. Acta 555 (1979) 436.
[6] T.J. McIntosh, S.A. Simon, D. Needham, C.H. Huang, Biochemistry 31 (1992) 2012.
[7] M. Kodama, H. Aoki, H. Takahashi, I. Hatta, Biochim. Biophys. Acta 1329 (1997) 61.
[8] M. Kodama, H. Kato, H. Aoki, Thermochim. Acta 353 (2000) 213.
[9] M. Kodama, H. Aoki, in: N. Garti (ed.) Surfactant Science Series 93: Thermal Behavior of Dispersed Systems, Marcel Dekker, New York, 2000, pp. 247–293.
[10] H. Aoki, M. Kodama, J. Thermal Anal. Calori. 64 (2001) 299.
[11] M. Kodama, H. Kato, H. Aoki, J. Thermal Anal. Calori. 64 (2001) 219.
[12] H. Aoki, M. Kodama, J. Biol. Phys. 28 (2002) 237.
[13] K. Miuram, M. Kawamoto, K. Inoue, M. Yamamoto, T. Kumasaka, M. Sugiura, A. Yamano, H. Moriyama, SPring-8 (Hyougo, Japan) User Experiment Report, 4 (2000) 168.
[14] C.R. Worthington, A.E. Blaurock, Biophys. J. 9 (1969) 970.
[15] D. Sayre, Acta Crystallogr. B. 5 (1952) 843.
[16] G.I. King, C.R. Worthington, Phys. Lett. 35A (1971) 259.
[17] J.F. Nagle, D.A. Wilkinson, Biophys. J. 23 (1978) 159.
[18] D.A. Wilkinson, J.F. Nagle, Biochemistry 20 (1981) 187.
[19] P.R. Maulik, D. Atkinson, G.G. Shipley, Biophys. J. 50 (1986) 1071.
[20] P.K. Sripada, P.R. Maulik, J.A. Hamilton, G.G. Shipley, J. Lipid Res. 28 (1987) 710.
[21] T.J. McIntosh, S.A. Simon, J.C. Ellington, N.A. Porter, Biochemistry 23 (1984) 4038.
[22] P.R. Maulik, G.G. Shipley, Biophys. J. 69 (1995) 1909.
[23] T.J. McIntosh, S.A. Simon, D. Needham, C.H. Huang, Biochemistry 31 (1992) 2012.